The Astrophysical Journal, 773:120 (6pp), 2013 August 20 doi:10.1088/0004-637X/773/2/120

CAN PLANETESIMALS FORM BY COLLISIONAL FUSION?

Dhrubaditya Mitra[1], J. S. Wettlaufer[1,2], and Axel Brandenburg[1,3]
[1] Nordita, KTH Royal Institute of Technology and Stockholm University, Roslagstullsbacken 23, SE-10691 Stockholm, Sweden
[2] Yale University, New Haven, CT, USA
[3] Department of Astronomy, AlbaNova University Center, Stockholm University, SE-10691 Stockholm, Sweden
Received 2012 November 26; accepted 2013 June 15; published 2013 August 1

ABSTRACT

As a test bed for the growth of protoplanetary bodies in a turbulent circumstellar disk, we examine the fate of a boulder using direct numerical simulations of particle seeded gas flowing around it. We provide an accurate description of the flow by imposing no-slip and non-penetrating boundary conditions on the boulder surface using the immersed boundary method pioneered by Peskin. Advected by the turbulent disk flow, the dust grains collide with the boulder and we compute the probability density function of the normal component of the collisional velocity. Through this examination of the statistics of collisional velocities, we test the recently developed concept of collisional fusion which provides a physical basis for a range of collisional velocities exhibiting perfect sticking. A boulder can then grow sufficiently rapidly to settle into a Keplerian orbit on disk evolution timescales.

Key words: accretion, accretion disks – planets and satellites: formation – protoplanetary disks – turbulence

Online-only material: color figures

1. INTRODUCTION

1.1. Accretion Disks and Protoplanets

Planet formation is hypothesized to occur through the growth of protoplanetary bodies formed from gas, dust, and ice grains in an accretion disk around a central star (Armitage 2010). The complex scenario of the planet formation process involves the following four stages. First, the initial collapse of interstellar gas to create the central protostar (∼0.1 Myr); second, the slow accretion of mass onto the star and the formation of primary planetesimals within the evolving accretion disk (∼Myr); third, a phase (∼Myr) of reduced accretion rate allowing the photoevaporative wind to divide the disk into an inner and an outer region at a radius determined by the ratio of the stellar accretion rate to the mass loss rate due to photoevaporation; and finally, there is a *clearing phase* (∼0.1 Myr) during which the inner disk accretes onto the star while the lightest elements of the outer disk are removed due to direct exposure to photoevaporative UV flux. Recent cosmochemical evidence reveals that the long held view of a ∼Myr age difference between Ca-Al-rich inclusions (CAIs) within carbonaceous chondrite meteorites and chondrules within chondrites can be refuted (Connelly et al. 2012). To the extent that these data demonstrate commensurability over disk lifetime scales of CAI and chondrule formation, the detailed transient development of matter within circumstellar disks becomes all the more compelling for studies that can isolate essential physical processes. Here we focus on fundamental aspects of the second stage above. This stage is crucial for understanding how the material that forms the building blocks of planets can organize into bodies that thwart the radiative pressure effects in the subsequent stages that sweep the disk of small particles and gas.[4]

The accretion disk is treated as a two-phase system defined by a fluid phase ("gas") and solid particles ("dust") advected by the fluid. Ubiquitous attractive long range van der Waals and electrostatic interactions facilitate the agglomeration and growth of small (micron or smaller) dust grains that are brought into proximity by the turbulent flow of the gas. However, depending on the material and the mechanical and thermodynamic conditions of a particle–particle collision, sticking (through a number of mechanisms), fragmentation, or bouncing will determine the fate and the size distribution of accreting matter from the small scales upward (Blum & Wurm 2008; Wettlaufer 2010; Zsom et al. 2011).

Because the central star creates a radially decaying pressure gradient, the gas moves at a slightly sub-Keplerian speed. Thus, depending on the position in the disk, there are a range of particle sizes that experience a strong "headwind" and so lose angular momentum, thereby driving them into the central star on timescales as rapidly as a century (Armitage 2010; Youdin 2010). We are concerned with the long-standing problem of how, when objects grow and begin to experience the local headwind, they can accumulate matter sufficiently quickly to slow their drift inward. To focus the question, we examine in some detail how a meter-sized object grows by accretion of small particles mediated by turbulent flows of the gas.

1.2. Hydrodynamic Preliminaries

The typical value of the "disk Mach number" $\mathcal{M}_d$ is based on the Keplerian velocity $v_{\rm kepler}$, which in the thin disk approximation is

$$\mathcal{M}_d = \frac{v_{\rm kepler}}{c_{\rm s}} \approx \frac{r}{h}, \qquad (1)$$

where r is the radial position in the disk and h is its vertical scale height. At 1 AU, $h/r \approx 0.02$ and hence $\mathcal{M}_d \approx 50$ (see, e.g., Armitage 2010, p. 40). Now, as noted above, because the central star creates a radially decreasing pressure gradient, relative to a meter-sized object the gas moves at a sub-Keplerian speed $v_{\rm wind} = \eta v_{\rm kepler}$ where η can be as small as 10^{-3} depending on the position in the disk.

To understand the effects of the interaction between the dust and the gas, we begin by considering a solid body of spherical shape with radius $R_{\rm SB}$, moving through a gas with kinematic

[4] A different hypothesis originally due to Safronov and Goldreich and Ward (see, e.g., Goldreich et al. 2004; Armitage 2010; Youdin 2010 for a review) leads to planetesimals by the gravitational collapse of the disk material. We do not consider this here.

viscosity ν and speed $v_{\rm wind}$. We estimate its Reynolds number as

$$\mathrm{Re}_{\rm SB} = \frac{v_{\rm wind} R_{\rm SB}}{\nu} = \frac{v_{\rm wind}}{c_{\rm s}} \frac{R_{\rm SB}}{\lambda} \frac{\lambda c_{\rm s}}{\nu} \approx \mathcal{M} \frac{R_{\rm SB}}{\lambda}, \quad (2)$$

where $\mathcal{M} \equiv v_{\rm wind}/c_{\rm s}$ is the Mach number of the headwind and λ is the mean-free-path of the gas molecules. Importantly, for this estimate we have used the well known expression for the viscosity of gases $\nu \sim c_{\rm s}\lambda$ (see, e.g., Lifshitz & Pitaevskii 1981, Section 8). Now, because $\mathcal{M} = \eta \mathcal{M}_d$, we can have $\mathcal{M} \approx 0.05$, and hence, so long as $R_{\rm SB} < \mathcal{M}^{-1}\lambda \approx 20\,\lambda$, the local Reynolds number of the solid body is less than unity. For $R_{\rm SB} \sim \lambda$ the size of the solid body is well below the smallest hydrodynamic length scale in the gas and its motion is then described by the simple drag law:

$$\frac{d\boldsymbol{v}_{\rm SB}}{dt} = \frac{1}{\tau_{\rm SB}} (\boldsymbol{v}_{\rm SB} - \boldsymbol{U}), \quad (3)$$

where $\boldsymbol{v}_{\rm SB}$ is the velocity of the particle, $\boldsymbol{U}$ is the local velocity of the gas, and $\tau_{\rm SB}$ is the so-called stopping time describing the deceleration of particle motion relative to the gas. When a particle is smaller than the typical hydrodynamic length scale in the problem, $\tau_{\rm SB}$ is given by the Epstein drag law,

$$\tau_{\rm SB}^{\rm Ep} = \frac{\rho_{\rm SB}}{\rho_{\rm g}} \frac{R_{\rm SB}}{c_{\rm s}}, \quad (4)$$

where $\rho_{\rm SB}$ is the material density of the solid particles and $\rho_{\rm g}$ is the gas density. When $\mathcal{M}^{-1}\lambda > R_{\rm SB} > \lambda$, the relevant drag law is that of Stokes and $\tau_{\rm SB}$ is given by

$$\tau_{\rm SB}^{\rm St} = \frac{2}{9} \frac{\rho_{\rm SB}}{\rho_{\rm g}} \frac{R_{\rm SB}^2}{\nu}. \quad (5)$$

Despite the fact that when $R_{\rm SB} > \mathcal{M}^{-1}\lambda$, the simple drag law (Equation (3)) no longer describes the motion of the dust particles, most numerical approaches to these problems (see, e.g., Johansen et al. 2007; Armitage 2010; Nelson & Gressel 2010; Carballido et al. 2010, 2011) continue to use it because a more accurate description is computationally prohibitive. Here we will call bodies of approximately this size "boulders." The mean-free-path λ in an accretion disk varies with radius; e.g., according to the minimum mass solar nebula model λ ranges from $\approx$10 cm at approximately 1.5 AU to $\approx$10 m at 10 AU. Hence $R_{\rm boulder}$ ranges from $\sim$2 m in inner disk regions to $\sim$200 m at about 10 AU. A more accurate approximation of the motion of such particles is given by the Maxey–Riley equation (Maxey & Riley 1983), which assumes a spherical geometry. While the Maxey–Riley approach is appealing on fundamental grounds, it has yet to be used in simulations of fully developed turbulence.

1.3. Bouncing, Sticking, Fusing

A crucial and often used assumption is that all collisions have a sticking probability of unity. Indeed, under such an assumption, planetesimal growth under a wide range of disk conditions is sufficiently rapid that there is no loss to the central star. Clearly, however, the probability of sticking depends, among other things, on the collisional velocity, the material properties of the colliding bodies, the ambient temperature, and the relative particle size. It is a commonly accepted picture that for collisional velocities V_c above a certain threshold value, $V_{\rm th} \sim$ 0.1–10 cm s^{-1}, particle agglomeration is not possible; and elastic rebound overcomes attractive surface and intermolecular forces (e.g., Chokshi et al. 1993). However, for bodies covered with ice, experimental (Blum & Wurm 2008) and theoretical (Wettlaufer 2010) studies of collisions between dust grains and meter-sized objects have elucidated the range of collisional velocities (which depends on the relative particle size) over which perfect sticking occurs. This latter work considers the basic role of the phase behavior of matter (phase diagrams, amorphs, and polymorphs) in leading to the so-called *collisional fusion*. In this fusion process, a physical basis for efficient sticking is provided through collisional melting/amphorphization/polymorphization and subsequent fusion/annealing to extend the collisional velocity range of sticking to $\Delta V_c \sim$ 1–100 m s$^{-1} \gg V_{\rm th}$, which encompasses both typical turbulent rms (root-mean-square) speeds and the velocity differences between boulders and small grains $\sim$1–50 m s^{-1}. Moreover, bodies of high melting temperature and multicomponent materials, such as silicon and olivine, can fuse in this manner depending on the details of their phase diagrams. Hence, in principle, the approach provides a framework for sticking from the inner to the outer nebula. Here, we explore the influence of such a range, ΔV_c, on the growth of a boulder in a simulated disk.

1.4. Summary of Approach

The fate of the boulder is studied from a reference frame fixed to it, while the gas flows around it. We provide an accurate description of the flow by performing a direct numerical simulation (DNS) with no-slip and non-penetrating boundary conditions on the boulder surface using a numerical technique called the Immersed Boundary Method (Peskin 2002). Hence, there is no ad hoc approximation involved in describing the mutual interaction between the boulder and the gas flow. However, at present, it is computationally prohibitive to solve for more than one boulder using this DNS scheme. Consequently, we focus our study on the flow mediated collisions between one boulder and many "effectively" point-sized dust grains whose sizes are much smaller than $R_{\rm boulder}$. Our principal approximations in treating the motion of the dust grains are (1) to use Equation (3) and (2) to ignore the back-reaction of the dust grains onto the flow. Advected by the turbulent disk flow, the dust grains collide with the boulder and we compute the probability density function (PDF) of the normal component of the collisional velocity.

2. MODEL

The mechanism of formation of planetesimals from dust grains is modeled by the same tools that are used to study, for example, hydrometeor growth in the terrestrial atmosphere, namely the coagulation/fragmentation equations of Smoluchowski (1916); see, e.g., Armitage (2010) for a recent review. The Smoluchowski equations are integro-differential equations that require two crucial ingredients: the probability distribution function of relative collisional velocities of the bodies in question and their sticking efficiency. The former, particularly for the inner disk region, is strongly influenced by turbulence. Recently, there has been significant progress in calculating the statistical properties of individual particle velocities (Carballido et al. 2011; Nelson & Gressel 2010) and, perhaps more importantly, pairwise relative velocities (Carballido et al. 2010) from DNSs. Similar results have also been obtained from both phenomenological (Ormel & Cuzzi 2007; Cuzzi & Hogan 2003) and shell (Hubbard 2012, 2013) models of turbulence.

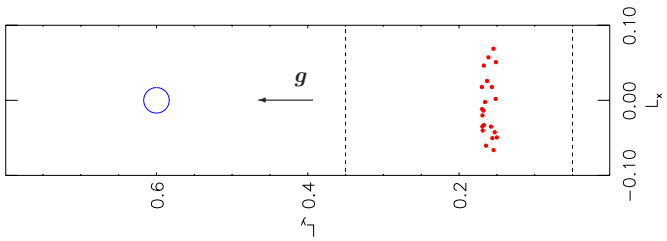

Figure 1. Illustration of our computational domain. The domain is divided into two halves. The left half contains the "boulder" sketched by the blue circle. In the right half the fluid is acted upon by an external white-in-time force which is non-zero only in the part of the domain limited by the two dashed lines. The turbulence thus generated is moved toward the "boulder" by the action of weak body force $\boldsymbol{g}$ along the arrow shown in the figure. The body force does not act directly on the particles, which are introduced continuously in a small area in the right half of the domain. Initial positions of a few particles are shown as red dots.

(A color version of this figure is available in the online journal.)

While these approaches provide key insights and intuition, they also leave open aspects with which the strategy we take is not burdened, such as (1) the use of the simple drag law (Equation (3)) to describe the motion of boulders, (2) the ability to obtain only the root-mean-square collision velocity, rather than the PDF of collision velocities (Carballido et al. 2010; Hubbard 2012, 2013 are exceptions), and (3) not modeling actual collisions, so that collisional velocities are inferred from looking at relative velocities at small distances. To calculate the PDF of collisional velocities between a boulder and small dust grains, such approximations may be too simplistic because of the presence of a boundary layer around the larger object. Indeed, Garaud et al. (2013) have recently pointed out the importance of using the PDF of collisional velocities instead of simply the root-mean-square value. However, taking this into account in a global (or even local) simulation of a disk is computationally prohibitive. Therefore, we take an initial modest step to try and understand such collisions by solving the equations of motion for weakly compressible fluids in two dimensions with a circular object—the boulder—inside. We ignore two classes of collisions: (1) between dust grains themselves and (2) between two or more boulders.

2.1. Numerical Method

Our computational domain is a rectangular box divided into two equal parts (Figure 1). In the right half, fluid turbulence is generated by external forcing that is non-zero between the two dashed lines shown in Figure 1. The turbulence thus generated is moved toward the "boulder" by the action of a body force $\boldsymbol{g}$ in the direction of the arrow shown in the figure. This body force is responsible for generating a mean flow, which models the headwind faced by a boulder—the circular object at the left half of the domain. The boundary layer around the boulder is fully resolved by imposing non-penetrating and no-slip boundary conditions using the immersed boundary method. After the flow has reached a stationary state, we introduce $N_{\rm p} = 2 \times 10^4$ particles into the right half of the domain as depicted in Figure 1. The motion of these particles obeys the simple drag law,

$$\frac{d\boldsymbol{v}_{\rm p}}{dt} = \frac{1}{\tau_{\rm p}}(\boldsymbol{v}_{\rm p} - \boldsymbol{U}), \tag{6}$$

with the characteristic drag time of the "dust particles" $\tau_{\rm p}$. As noted before and as is clear from context, no such assumption need be made for the boulder. The back-reaction from the dust grains to the gas is ignored. When a dust grain collides with the boulder it is removed from the simulation and a new dust grain is introduced in the right half of the domain. We use the Pencil Code[5] in which the immersed boundary method was implemented by Haugen & Kragset (2010).

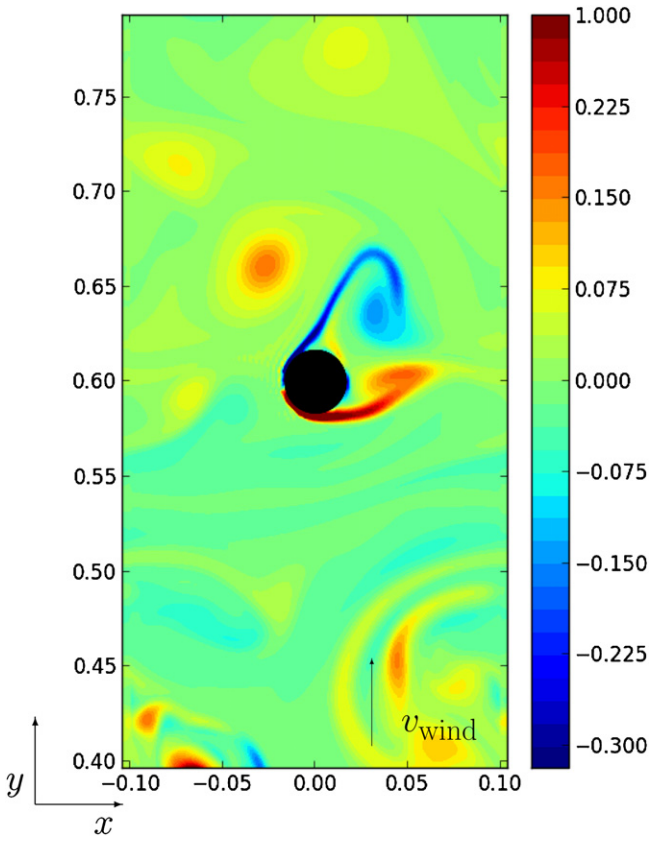

Figure 2. Contour plot of vorticity in the upper half of our domain. The black circle at the center of the domain is the circular object. The arrow shows the time- and space-averaged direction of $v_{\rm wind}$.

(A color version of this figure is available in the online journal.)

2.2. Parameters

The characteristic large-scale velocity is the root-mean-square velocity in the streamwise direction, $v_{\rm wind} \equiv \langle v_y^2 \rangle^{1/2}$. We always use the Reynolds number corresponding to the central solid body, defined by

$$\mathrm{Re}_{\rm SB} \equiv v_{\rm wind} R_{\rm SB}/\nu. \tag{7}$$

The Stokes number of the "dust particles" is defined by

$$\mathrm{St} \equiv \tau_{\rm p}/\tau_{\rm L}, \tag{8}$$

where $\tau_{\rm L} = L_y/v_{\rm wind}$, with L_y being the length of our domain along the streamwise direction; from right to left in Figure 1. By virtue of limiting our simulations to two dimensions, we can access a larger range of particle Reynolds numbers $\mathrm{Re}_{\rm SB}$, from 30 to 1000 with resolutions ranging from 128×512 to 512×2048 grid points. The surface of the boulder is resolved with 100–400 grid points.

3. RESULTS

A representative snapshot of the vorticity field is given in Figure 2. A movie, available online at http://www.youtube.com/

[5] http://pencil-code.googlecode.com/

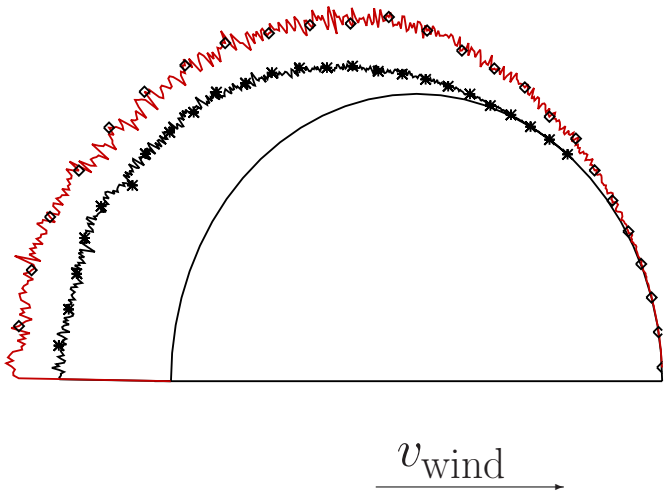

Figure 3. Plot showing how the boulder would grow if all collisions were perfectly sticky. The arrow shows the direction of $v_{\rm wind}$. The growth for two different runs (1) $\mathrm{Re_{SB}} \approx 29$, $\mathrm{St} \approx 0.5$ (∗), and (2) $\mathrm{Re_{SB}} \approx 1000$, $\mathrm{St} \approx 0.6$ (□), for the same total time duration is shown. The inner semi-circle shows the initial surface of the boulder.

(A color version of this figure is available in the online journal.)

watch?v=-Fr5Q2Kp0wo, shows that, although over a spatiotemporal average there is a streamwise mean flow on the boulder, there are large fluctuations. At a particular instant the direction of the gas velocity at the boulder surface can deviate significantly from the streamwise direction. Furthermore, we observe that most of the collisions do not occur at the front face of the boulder but there are a significant number of collisions that deviate from centrality; see Figure 3. Note, however, that there are almost no collisions on the backside of the boulder. A clear implication of this is that, for perfect sticking of all collisions, an initially spherical boulder evolves into a non-spheroidal body and hence may begin to tumble in the disk.

3.1. PDF of Collisional Velocities

The criterion for a collision is that the distance between a dust grain and the boulder becomes less than a grid point. After this collision, we remove the dust grain from the simulation. For $\mathrm{Re_{SB}} \approx 1000$ in Figure 4, we plot the PDF, $P(v_{\rm n})$, of the component of the velocity of the dust grain normal to the surface of the boulder, v_n. At small v_n, $P(v_{\rm n}) \sim v_{\rm n}^2$ (Figure 4(a)) and at large v_n the falloff is $\sim \exp[-(v_{\rm n}/v_0)^2]$ (Figure 4(b)). However, as shown in Figure 4(c), over the whole range it is difficult to fit the PDF with a Maxwellian distribution.

Now we consider how the PDF changes as the Stokes and Reynolds numbers of the flow change. We vary the Reynolds number by changing the viscosity of the flow. Hence, a change in Reynolds number also changes $v_{\rm wind}$, and this leads to a change in the Stokes number.[6] Therefore, in our approach to the numerical treatment of the flow, it is not possible to perform a systematic study of the Reynolds number dependence of the PDF at the fixed Stokes number. However, in order to produce an effective treatment of such a circumstance, we present in Figure 5 the PDFs for different Reynolds numbers wherein the Stokes numbers are not too different from each other. We see that for small $\mathrm{Re_{SB}}$ the peak of the PDF lies very close to $v_{\rm wind}$, but as $\mathrm{Re_{SB}}$ increases the peak moves to smaller velocities by

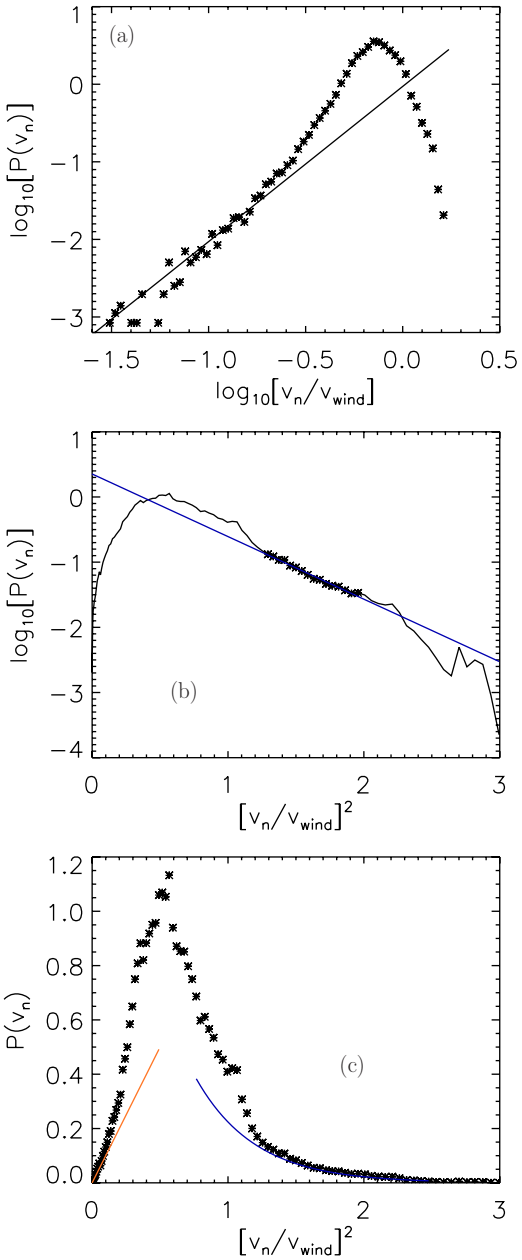

Figure 4. PDF of collisional velocities for $\mathrm{Re_{SB}} \approx 1000$, $\mathrm{St} \approx 0.6$. (a) Log–log (base 10) plot for small v_n; $P(v_{\rm n}) \sim (v_{\rm n}/v_{\rm wind})^2$, the straight line has a slope of 2. (b) Semi-log (base 10) at large v_n. The straight line, which is a fit to the points denoted by the symbol ∗, has slope −0.96. (c) The PDF with the two approximations at small and larger v_n plotted together.

(A color version of this figure is available in the online journal.)

only a very small amount. Although $\mathrm{Re_{SB}}$ changes by almost a factor of 20, the position of the peak (normalized by $v_{\rm wind}$) only changes from 0.6 to 0.3. A more dramatic change is observed in the PDF as the Stokes number is changed from 0.5 to 0.1 when $\mathrm{Re} \approx 29$ is held fixed, as shown in Figure 6. In particular, the tail of the PDF at high v_n is severely cutoff as the Stokes number is decreased by a factor of five. One can understand this as follows: when the Stokes number decreases, the dust grains begin to follow streamlines and hence never collide with the boulder. The implication of this is clearly that a *smaller Stokes number* implies a *smaller number of high-impact collisions*. Nevertheless, the most striking result for the problem at hand is the insensitivity of the PDF to $\mathrm{Re_{SB}}$ and St.

[6] As we change viscosity holding all other variables, including the body force $\boldsymbol{g}$, constant, $v_{\rm wind}$ also changes. This changes $\tau_{\rm L} = L_y/v_{\rm wind}$ which consequently changes St through Equation (8).

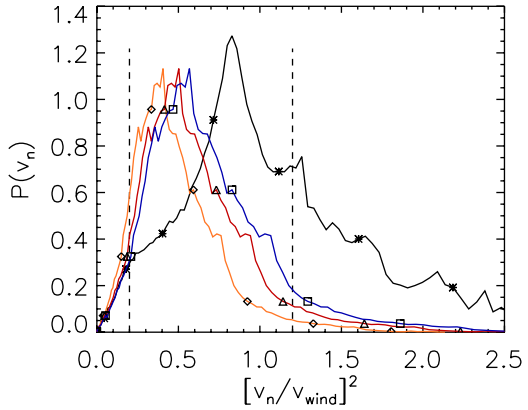

Figure 5. Probability distribution function, $P(v_n)$, of the normal component of collisional velocity vs. $(v_n/v_{\rm wind})^2$ for four different runs: (a) $\mathrm{Re_{SB}} \approx 29$, $\mathrm{St} \approx 0.5$ (∗), (b) $\mathrm{Re_{SB}} \approx 69$, $\mathrm{St} \approx 1$ (□), (c) $\mathrm{Re_{SB}} \approx 516$, $\mathrm{St} \approx 0.7$ (△), and (d) $\mathrm{Re_{SB}} \approx 1000$, $\mathrm{St} \approx 0.6$ (◇).

(A color version of this figure is available in the online journal.)

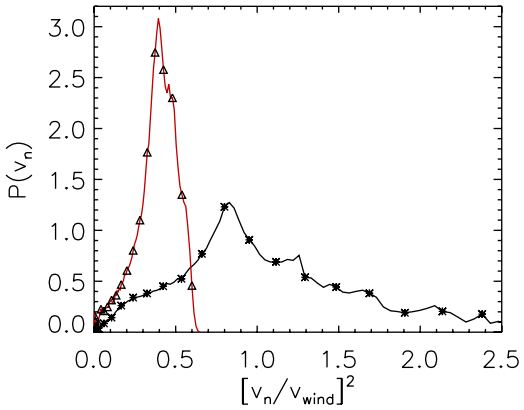

Figure 6. Probability distribution function, $P(v_n)$, of normal component of collisional velocity vs. $[v_n/v_{\rm wind}]^2$ for two different Stokes numbers; $\mathrm{St} \approx 0.5$ (∗), and $\mathrm{St} \approx 0.1$ (△), for $\mathrm{Re_{SB}} \approx 29$.

(A color version of this figure is available in the online journal.)

3.2. From DNS to Disk Astrophysics

Our simulations take place in the reference frame of the boulder. Although the boulder is also comoving with the local gas with velocity $v_{\rm kepler}$, it is the head wind, which corresponds to $v_{\rm wind}$ in our simulations, that sets the velocity scale. The radius of the boulder is taken to be ≈10 m. The magnitude of the headwind in the disk is estimated to be $v_{\rm wind} \approx 10^{-3} v_{\rm kepler} \approx 3 \times 10^3\,\mathrm{cm\,s^{-1}}$ (see, e.g., Armitage 2010, p. 130). In the astrophysical literature it is common to non-dimensionalize $\tau_{\rm p}$ with $\Omega_{\rm kepler}$, the Keplerian frequency, to define the orbital Stokes number, $\mathrm{St_{kepler}}$. Here, we use the largest eddy timescale $\tau_{\rm L} = L_y/v_{\rm wind}$, to obtain St. These two Stokes numbers are related by

$$\mathrm{St_{kepler}} = \mathrm{St}\frac{\tau_L}{\tau_{\rm orb}}, \tag{9}$$

where $\tau_{\rm orb}$ is the characteristic timescale of the Keplerian orbit defined by

$$\tau_{\rm orb} = \frac{R_{\rm orb}}{v_{\rm kepler}}, \tag{10}$$

where $R_{\rm orb}$ is the orbital radius. Using the definition of the two timescales $\tau_{\rm L}$ and $\tau_{\rm orb}$, we obtain the ratio of the two Stokes numbers to be

$$\frac{\mathrm{St_{kepler}}}{\mathrm{St}} = \frac{L_y}{R_{\rm orb}}\frac{v_{\rm kepler}}{v_{\rm wind}} \approx 10^{-5}, \tag{11}$$

where we have used $R_{\rm orb} = 1\,\mathrm{AU}$, $L_y = 50 R_{\rm SB} \approx 500$ meter, and $v_{\rm wind} = \eta v_{\rm kepler}$ with $\eta = 10^{-3}$. We have used the Stokes number ranging from $\mathrm{St} = 0.1$ to 2 which in turn gives $\mathrm{St_{kepler}} \approx 10^{-6}$ to 2×10^{-5}. We use the same conventions used in the supplementary information of Johansen et al. (2007) to convert the value of $\mathrm{St_{kepler}}$ to a radius of the dust grain; this implies that our "dust particles" are of the size of tenths of millimeters or smaller. Clearly, the "dust particles" are smaller than hydrodynamic scales, and hence it is justified to consider them as point objects whose motions are described by the Epstein drag law.

3.3. Collisional Fusion

The PDFs of collisional velocities show that, irrespective of the Reynolds number and the Stokes number within the range considered by us, most collisions occur at velocities rather near to $v_{\rm wind}$. To illustrate this, in Figure 5 we have drawn two vertical dashed lines at $(v_{\rm n}/v_{\rm wind})^2 = 0.2$ and $v_{\rm n}/v_{\rm wind} = 1.2$. The area under the PDF between the two lines includes approximately 95% of the total number of collisions. Translated to parameters in the disk, this implies that, if there is a mechanism by which dust grains with velocities ranging from $0.4\,v_{\rm wind}$ to $1.1\,v_{\rm wind}$ would stick to a boulder, then we could consider 95% of collisions to have a perfect sticking probability.

Roughly speaking, this implies a range of velocities 6–36 $\mathrm{m\,s^{-1}}$. These collisional velocities are far too high for the bodies to fuse by attractive intermolecular forces. An alternative scenario by which the colliding bodies can fuse at high speed has been suggested by Wettlaufer (2010). As discussed in Section 1.3, the very high local pressures that occur during a collision can lead to phase change. If, when the pressure begins to relax during rebound the momentarily liquified (or disordered) interfacial material re-freezes (or anneals) before particle separation, then fusion can occur. The idea was demonstrated when the colliding bodies are covered by ice, but the theory is generally applicable to all materials whose phase diagram is known in detail. An example of the process in a high melting temperature material (silicon) was noted in Wettlaufer (2010). Hence, whether the range of collisional velocities over which such process can occur in a material such as olivine matches with the range we find here is a topic of ongoing research. Note that here the particle Reynolds number $\mathrm{Re_{SB}}$ varies linearly with the particle radius but the range over which most of the collisions occur does not depend sensitively on $\mathrm{Re_{SB}}$, and hence not on the particle radius. Thus, runaway growth of the boulder through the accretion of dust grains is a viable mechanism in areas of the disk where collisional fusion can operate in the range we obtain.

4. DISCUSSION AND CONCLUSION

To describe the motion of micron-sized dust grains in a protoplanetary disk the simple drag law of Equation (6) is sufficient. Theoretical estimates (see, e.g., Armitage 2010, p. 120) suggest that micron-sized dust particles in the inner disk (about 5 AU) can grow up to a size of tens of centimeters if we assume that the presence of turbulence increases the number of collisions and that almost all collisions result in coagulation by long-ranged intermolecular forces. But the process that allows

them to continue to grow to the size of planetesimals is not well understood. As the dust grains grow, at some stage they become boulders and their local Reynolds number exceeds unity. At this stage we need a more accurate description of their interaction with the gas than the one provided by Equation (3). Here we provide such a description of a boulder colliding with dust grains by using the immersed boundary method of Peskin (2002). Remarkably, we find that the PDF of collisional velocities depends weakly on $\mathrm{Re_{SB}}$ and St. In particular, we find that, if collisional fusion between dust grains is possible in the range of collisional velocities ΔV_c between 0.4 and 1.1 v_{wind}, then approximately 95% of the collisions exhibit perfect sticking and runaway growth of a boulder to a planetesimal is possible. Whether collisional fusion can occur in this range is a problem of material science under extreme conditions and is the subject of ongoing research in a future paper.

Recent studies (Garaud et al. 2013; Windmark et al. 2012) have pointed out that the PDF of collisional velocities is a crucial ingredient to the coagulation-fragmentation models. In particular, Windmark et al. (2012) have assumed the PDF of collisional velocities to be Maxwellian, and have concluded that, by virtue of considering a PDF that is continuous at small values of its argument, growth by sticking is possible even if the sticking efficiency is determined by long-ranged intermolecular forces (sticking with efficiency unity if the relative velocity of collisions is less than 5 cm $\mathrm{s^{-1}}$). Here, we determine numerically the PDFs for the classes of collisions between boulders and dust grains and find that it cannot be simply described by a Maxwellian distribution—although it does have an exponential tail. It is well known that in turbulent flows the PDF of the velocities of a tracer particle is Gaussian. We do not know of any study of the PDF of the velocity of inertial particles (particles that obey Equation (6)) in turbulent flows, but it is reasonable to assume that it would also be Gaussian. If such an assumption holds, then we expect the PDF of collisional velocities to have an exponential tail, so long as the size of particles is not comparable. Were the colliding particles to be of roughly the same size, the PDF may indeed have a power-law tail by virtue of intermittency.

In an earlier paper, Sekiya & Takeda (2003) found that dust monomers advected by a steady laminar flow do not collide with a spherical solid body with a radius much larger than the hydrodynamic length scale. The crucial limitation in their work was to assume the flow to be laminar. Here, we have considered turbulent flow and have obtained a different result, i.e., a significant percentage of the dust particles do hit the solid body with the PDF of collisional velocities peaking around the speed of the head wind.

There exists an alternative scenario of planetesimal formation (Johansen et al. 2007) in which the boulders are described by the simple drag law (Equation (3)) but their back-reaction on the gas is accounted for. This is predicted to give rise to "streaming instabilities" which form boulder clusters around high pressure regions. Such clusters are then expected to coagulate by mutual gravitational interaction. In the light of the arguments presented in the present paper, this streaming instability scenario requires further investigation. This is because basic physical principles tell us that the description of the motion of the boulder is inadequately described by Equation (3). While the immersed boundary method can potentially solve this problem, we need to have massive computational resources to examine the fate of many boulders.

We conclude by pointing out the limitations of our study. First, here we confine ourselves to two dimensions. On the one hand, this has the virtue of permitting a larger range of $\mathrm{Re_{SB}}$ that can be easily accessed numerically. On the other hand, we cannot capture the richness of particle fusion in the remaining dimension. However, we believe that this may imply that the growth of the particle we have studied to be a lower bound. Second, when collisional fusion starts operating the initial spherical object we study will not remain spherical. This may quantitatively affect further growth in a manner that depends on how the boulder tumbles through the disk. Third, the turbulence in our flow is generated by external forcing. It would be appropriate to use shearing-box simulations in three dimensions where the flow is driven by magneto-rotational instability. We believe that these rather clear limitations do not detract from the robust results obtained in this study, which clarify the microphysical questions for a range of colliding materials and the computational fluid dynamics issues that will advance a sober assessment of planetesimal formation processes.

Financial support from the European Research Council under the AstroDyn Research Project 227952, and the Swedish Research Council grant 2011-5423 is gratefully acknowledged. J.S.W. thanks the Wenner-Gren and John Simon Guggenheim Foundations, and the Swedish Research Council. We also thank the anonymous referee for useful suggestions, and N. Haugen and O. Gressel for useful discussions.

REFERENCES

Armitage, P. J. 2010, Astrophysics of Planet Formation (Cambridge: Cambridge Univ. Press)
Blum, J., & Wurm, G. 2008, ARA&A, 46, 21
Carballido, A., Bai, X.-N., & Cuzzi, J. N. 2011, MNRAS, 415, 93
Carballido, A., Cuzzi, J. N., & Hogan, R. C. 2010, MNRAS, 405, 2339
Chokshi, A., Tielens, A. G. G. M., & Hollenbach, D. 1993, ApJ, 407, 806
Connelly, J., Bizzarro, M., Krot, A., et al. 2012, Sci, 338, 651
Cuzzi, J. N., & Hogan, R. C. 2003, Icar, 164, 127
Garaud, P., Meru, F., Galvagni, M., & Olczak, C. 2013, ApJ, 764, 146
Goldreich, P., Lithwick, Y., & Sari, R. 2004, ARA&A, 42, 549
Haugen, N. E. L., & Kragset, S. 2010, JFM, 661, 239
Hubbard, A. 2012, MNRAS, 426, 784
Hubbard, A. 2013, MNRAS, 432, 1274
Johansen, A., Oishi, J. S., Mac Low, M.-M., et al. 2007, Natur, 448, 1022
Lifshitz, E. M., & Pitaevskii, L. P. 1981, Physical Kinetics, Vol. 10 (Course of Theoretical Physics; Oxford: Pergamon)
Maxey, M. R., & Riley, J. J. 1983, PhFl, 4, 883
Nelson, R. P., & Gressel, O. 2010, MNRAS, 409, 639
Ormel, C. W., & Cuzzi, J. N. 2007, A&A, 466, 413
Peskin, C. 2002, AcNum, 11, 479
Sekiya, M., & Takeda, H. 2003, EP&S, 55, 263
Smoluchowski, M. V. 1916, ZPhy, 17, 557
Wettlaufer, J. S. 2010, ApJ, 719, 540
Windmark, F., Birnstiel, T., Ormel, C. W., & Dullemond, C. P. 2012, A&A, 544, L16
Youdin, A. 2010, in EAS Publications Series, Vol. 41, Physics and Astrophysics of Planetary Systems, ed. T. Montmerle, D. Ehrenreich, & A.-M. Lagrange (Les Ulis, France: EDP Sciences), 187
Zsom, A., Ormel, C., Dullemond, C., & Henning, T. 2011, A&A, 534, A73